Interface interactions driven antioxidant properties in olive leaf extract/cellulose nanocrystals/poly(butylene adipate-co-terephthalate)

International Journal of Biological Macromolecules 272 (2024) 132509

Contents lists available at ScienceDirect

International Journal of Biological Macromolecules

journal homepage: www.elsevier.com/locate/ijbiomac

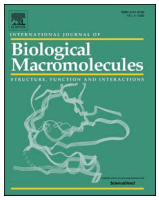

Interface interactions driven antioxidant properties in olive leaf extract/cellulose nanocrystals/poly(butylene adipate-*co*-terephthalate) biomaterials

Giuseppa Anna De Cristofaro [a], Marina Paolucci [a], Daniela Pappalardo [a], Caterina Pagliarulo [a], Valentina Sessini [b], Giada Lo Re [c,d,*]

[a] University of Sannio - Department of Science and Technology, Via Francesco De Sanctis snc, 82100 Benevento, Italy
[b] Department of Organic and Inorganic Chemistry, Institute of Chemical Research "Andrés M. del Río" (IQAR), Universidad de Alcalá, Campus Universitario, 28871 Alcalá de Henares, Madrid, Spain
[c] Department of Industrial and Materials Science, Chalmers University of Technology, Rännvägen 2A, 41258 Gothenburg, Sweden
[d] Wallenberg Wood Science Centre, Chalmers University of Technology, Kemigården 4, 41258 Gothenburg, Sweden

ARTICLE INFO

Keywords:
Agricultural waste
Oleuropein
Biodegradable packaging
Cellulose nanocrystals
Fluorescence spectroscopy

ABSTRACT

Functional packaging represents a new frontier for research on food packaging materials. In this context, adding antioxidant properties to packaging films is of interest. In this study, poly(butylene adipate-*co*-terephthalate) (PBAT) and olive leaf extract (OLE) have been melt-compounded to obtain novel biomaterials suitable for applications which would benefit from the antioxidant activity. The effect of cellulose nanocrystals (CNC) on the PBAT/OLE system was investigated, considering the interface interactions between PBAT/OLE and OLE/CNC. The biomaterials' physical and antioxidant properties were characterized. Morphological analysis corroborates the full miscibility between OLE and PBAT and that OLE favours CNC dispersion into the polymer matrix. Tensile tests show a stable plasticizer effect of OLE for a month in line with good interface PBAT/OLE interactions. Simulant food tests indicate a delay of OLE release from the 20 wt% OLE-based materials. Antioxidant activity tests prove the antioxidant effect of OLE depending on the released polyphenols, prolonged in the system at 20 wt % of OLE. Fluorescence spectroscopy demonstrates the nature of the non-covalent PBAT/OLE interphase interactions in π-π stacking bonds. The presence of CNC in the biomaterials leads to strong hydrogen bonding interactions between CNC and OLE, accelerating OLE released from the PBAT matrix.

1. Introduction

Among the harmful substances to which living beings are exposed, plastics certainly occupy a prominent place. Plastics and its fragments, also defined as micro and nanoplastics, depending on the size, are worldwide spread as they can be found in marine and freshwater [1], food [2] and in many human tissues [3–5], even placenta [6]. Since conventional plastics are not biodegradable, when the application does not require durability, their replacement with biodegradable plastics can substantially reduce the environmental impact of plastic waste.

According to the latest market data compiled by European Bioplastics, the production of biodegradable plastics will increase to about 3.5 million tons in 2027, because of their ever-increasing number of applications on the market, from packaging to electronics, agriculture, and textile [7]. However, packaging remains the most relevant market segment for bioplastics, absorbing around 48 % of the total bioplastic market in 2022 [7].

Among thermoplastic aliphatic polyesters, poly(lactic acid) (PLA) and poly(hydroxyalkanoates) (PHAs) are the most relevant examples of biodegradable polymers obtained from renewable resources. However, their relatively high cost, brittleness, and poor melt processability limit their applications [8]. Although not fully bio-sourced, poly (butylene adipate-*co*-terephthalate) (PBAT) is one of the most suitable biodegradable thermoplastics for low density polyethylene (LDPE) replacement, thanks to its similar mechanical properties and easy melt processability. PBAT is an aliphatic/aromatic random *co*-polyester, fully

* Corresponding author at: Department of Industrial and Materials Science, Chalmers University of Technology, Rännvägen 2A, 41258 Gothenburg, Sweden.
E-mail addresses: gadecristofaro@unisannio.it (G.A. De Cristofaro), paolucci@unisannio.it (M. Paolucci), pappal@unisannio.it (D. Pappalardo), pagliarc@unisannio.it (C. Pagliarulo), valentina.sessini@uah.es (V. Sessini), giadal@chalmers.se (G. Lo Re).

https://doi.org/10.1016/j.ijbiomac.2024.132509
Received 22 February 2024; Received in revised form 12 May 2024; Accepted 17 May 2024
Available online 5 June 2024

compostable, obtained from the condensation of 1,4-butanediol, adipic acid and terephthalic acid. The aliphatic portion of PBAT provides good melt processability while the aromatic one confers good mechanical properties [9]. Compared to most biodegradable polyesters such as PLA and PHAs, PBAT is more flexible and therefore holds great promise for a wide range of potential applications. By 2026, PBAT is projected to account for 30 % of global bioplastics production capacity [10]. Furthermore, PBAT has been presented as biodegradable material that releases no toxic metabolites and causes no harmful effects to the environment [11].

Due to its excellent stretchability and melt strength, PBAT has demonstrated to be a good candidate for film manufacturing in food packaging or in outdoor applications such as mulching films [9]. However, when employed to manufacture functional films, the addition of different molecules can influence the PBAT inherent processability and mechanical performance [12].

In recent decades the concept of "functional packaging" has represented a new frontier for research on food packaging materials. Compared to classic packaging that does not interact with food, functional packaging involves an interaction between the packaging material and the food products. The interaction is allowed by the presence of substances that act on food with their positive effects and preserving their organoleptic properties [13,14]. Moreover, the use of functional mulching films is relevant also for agriculture to reduce the soil contact and weathering of vegetables or some fruits, such as berries [15].

As well, the use of natural substances added to functional packaging for food preservation or mulching films responds not only to the needs of the consumer but also to those of the environment [16].

In this contest, phytochemicals are naturally occurring compounds in plants which offer various beneficial properties for human health [17–19]. In addition to their well-known antioxidant properties, many phytochemicals have other functional and preservative functions that may be of interest for both human health and biotechnological applications [20,21]. Waste or by-products of the agri-food chain are rich in phytochemicals, and bioactive molecules, thus, extracts from these materials can be utilized in food, nutraceuticals, pharmaceuticals, and cosmetics industries, as well as in agriculture and environmental applications such as in bioplastics [22,23]. Furthermore, using these agri-food chain by-products allows to reduce the amount of waste, transforming them into value-added products [24].

Italy is only second to Spain in the global production of olive oil [25,26]. This agricultural activity generates, at any step of production, an enormous amount of waste, from olive mill wastewater to leaves. Such waste is rich in bioactive molecules, mainly polyphenols, and plant secondary metabolites with a high number of hydroxyl groups responsible for the well-known antioxidant properties [27–29]. The main polyphenols in the olive oil chain by-products are hydroxytyrosol, tyrosol, and oleuropein [30,31].

In the last few decades, the use of natural polyphenols has been reported for the protection of the polymeric matrix, slowing down its degradation in oxidative condition, such as weather exposure [32–35]. Up to now, relatively few studies have been carried out on PBAT films functionalized with polyphenols or plant extracts, however, all of them indicate that the interactions lead to a modification of PBAT properties [36–40], often related to a PBAT plasticization and embrittlement. The bioactive molecules are thermosensitive and keen to phase separate from the matrix, leading to the ageing and consequent mechanical properties decay of the PBAT films. To prevent a possible ageing of the functional PBAT films by limiting the migration and the thermosensitivity of the active biomolecules, we evaluate the absorption of the water-soluble bioactive molecules into hydrophilic cellulose, prior their melt compounding.

In the realm of biomaterials, cellulose is the most abundant, renewable natural polymer. Cellulose nanocrystals (CNC) are relatively low cost and renewable nanomaterials, currently commercially available, obtained by extraction from cellulose fibres by strong acid hydrolysis [41–43]. CNC possesses unique properties, combining high strength and stiffness to relatively light weight and biodegradability. Therefore, CNC have been applied as filler in polymeric matrices aiming to their reinforcement and enhancing their sustainability and eco-friendly character for various applications [44,45].

In this study we focus on the incorporation of bioactive molecules extracted from the waste of olive oil production, in particular the olive leaf extract (OLE), to produce biodegradable PBAT functional packaging by melt processing that can be used in food or agricultural applications, as already studied for different matrices [34,46–48].

The OLE extract, which are mainly composed by polyphenols, could generate interactions with the aromatic part of PBAT, derived from the terephthalic acid, (*i.e.* π-π interactions), eventually modulating the release of OLE from the polymeric matrix. Under the rationale of exploit the potential chemical interactions between and between OLE and PBAT and OLE and CNC, we prepared also OLE/CNC/PBAT biomaterials.

Due to its polysaccharide nature, the hydrophilic CNC could not only support the homogeneous dispersion of the OLE in the films, but possibly reduce the burst release of hydrophilic OLE from the polymeric matrix, *via e.g.*, hydrogen bond interactions. Therefore, we absorbed OLE into never dried CNC, enabling a wet feeding procedure for the melt compounding of PBAT-based biomaterials. The wet feeding prevents CNC irreversible agglomeration, *i.e.*, hornification, upon drying, for enhancing the dispersion of the CNC in PBAT, which is not sensible to hydrolytic degradation [49–51].

The physical and antioxidant properties of the films were investigated to validate their possible use in food packaging or in outdoor mulching application.

2. Materials and methods

2.1. Materials

PBAT (Ecoworld® 003) was purchased from Jinhui ZhaoLong High Technology Co. Ltd. (China), with a declared density of 1.26 g/cm^3 and a melt flow rate $\leq$ 5 g/10 min (ISO 1133) at 190 °C and 2.16 kg. Water dispersion (8 wt% solid content) of sulfuric acid-hydrolyzed CNC was purchased from CelluForce, Canada. OLE was obtained from aqueous microwave extraction of olive leaves kindly furnished by Oleificio Vascello (Morcone, Benevento, Italy). 2,2-Diphenyl-1-picrylhydrazyl (DPPH), dimethyl sulfoxide (DMSO) and ethanol (EtOH) were supplied by Sigma-Aldrich.

2.2. Olive leaves extract preparation and characterization

Olea europaea leaves, Ortice variety were cleaned by dust and debris, air dried for 10 days and then shredded to fine powder. The powder was extracted by means of a household microwave set at 300 W for 2 min, using distilled water as solvent (1:25 w:v). The extract was cooled and filtered with a Whatman Chromatography paper (WHA3001861), then frozen at −80 °C and freeze-dried by Lio—5P.

OLE was characterized by Attenuated total reflectance Fourier transform infrared (ATR-FTIR) using a PerkinElmer FT-IR Spectrometer Frontier in ATR mode. 20 scans were performed from 4000 to 400 cm^{-1} with a resolution of 4 cm^{-1}. All data were treated using PerkinElmer Spectrum software. It is worth noting that further structural analyses of the extract in comparison with the olive leaves of different species, collected in different periods of the year, were previously reported [30].

2.3. Biomaterials preparation: melt processing

Biomaterials based on PBAT containing freeze-dried OLE as antioxidant and/or CNC were processed using a micro-compounder (15HT XPLORE, The Netherlands) at 125 °C and 60 rpm for 5 min. OLE was added at the concentrations of 10 wt% and 20 wt% directly to the polymeric matrix to obtain 10-OLE-PBAT and 20-OLE-PBAT. When CNC

were used, OLE was previously mixed with 10 wt% of CNC powder dissolved in 30 wt% of water and then the OLE-CNC compound was inserted into the extruder together with the PBAT to produce 10-OLE-CNC-PBAT and 20-OLE-CNC-PBAT. The obtained biomaterials are reported in Table 1. A biomaterial containing only 10 wt% CNC was also produced to be used as a reference for thermal analysis (CNC-PBAT). Biomaterials were shaped in Dumbbell's specimens and bars by injection moulding in a micro-injection moulding machine (Xplore, The Netherlands). The temperature for the injection was set at 130 °C for the melt, and at 23 °C for the mould. The injection pressure followed 3 steps: 2 steps at 15 bar for 5 s and 1 step at 15 bar for 3 s. The samples obtained were used for mechanical, thermal and release tests. The thermal analysis was repeated after 15 days on aged samples while the tensile characterization was performed on aged samples after 15 days and 1 month, stored at room temperature in a cool and dry place in aluminium paper to avoid light damage.

2.4. Differential scanning calorimetry (DSC)

Thermal properties were characterized by DSC analysis using a DSC2 star system, Mettler Toledo. Approximately 1–5 mg of biomaterial were sealed in aluminium pans while an empty pan was used as reference. The analysis method was composed by an isotherm step at 30 °C for 1 min followed by a heat-cool-heat program under nitrogen atmosphere (50 ml/min); a first heating scan from 30 °C to 160 °C or 200 °C at 10 °C/min ending with an isotherm for 1 min, a cooling scan from 160 °C or 200 °C to −80 °C at 10 °C/min followed by an isotherm at −80 °C for 2 min, and finally a second heating scan from −80 °C to 160 °C or 200 °C at 10 °C/min. The glass transition (T_g) and the melting temperatures (T_m) were calculated from the second heating scan while the crystallization temperature (T_c) from the cooling scan. The crystallinity of the samples was calculated according with Eq. (1).

$$\chi^a = \frac{1}{x^a}\left[\frac{\Delta H_m}{\Delta H_{m0}}\right]\cdot 100 \quad (1)$$

χ^a represents the degree of crystallinity of the component a, ΔH_m is the melting enthalpy, ΔH_{m0} is the melting enthalpy for a 100 % crystalline material while x^a is the percentage of the PBAT in the sample. The value used for ΔH_{m0} of PBAT was 114 J/mol [52].

2.5. Thermogravimetric analysis (TGA)

1–10 mg of biomaterial in alumina crucible, previously conditioned at 54 % RH for 24 h, were analysed for their thermal stability using a thermogravimetric analyser (TGA/DSC 3^+ Star System). Analysis method involved an isotherm at 25 °C for 1 min; a first heating from 25 °C to 70 °C with an increase of 10 °C per minute (10 °C/min); an isotherm at 70 °C for 15 min and a second heating from 70 °C to 500 °C (5 °C/min). The analysis was performed under nitrogen flow (50 mL/min). The onset degradation temperature ($T_{5\%}$) was recorded at mass loss value of 5 % while the char percentage was recorded at the maximum temperature of analysis. The temperature at which the maximum degradation rate occurred (T_d) was identified from the peak in the first derivative.

Table 1
Composition of biomaterials based on PBAT and filled with OLE and CNC. Initial water content (before melt processing) was 30 g per 100 g of biomaterial (30 ppb) produced by wet feeding. Water evaporated during the extrusion process.

Acronym	PBAT [wt %]	OLE [wt %]	Dried CNC [wt%]	Initial [ppb]/final [wt%] water
PBAT	100	0	0	30/2 ± 1
CNC-PBAT	90	0	10	30/2 ± 1
10-OLE-PBAT	90	10	0	30/2 ± 1
10-OLE-CNC-PBAT	80	10	10	30/2 ± 1
20-OLE-PBAT	80	20	0	30/2 ± 1
20-OLE-CNC-PBAT	70	20	10	30/2 ± 1

2.6. Tensile test

The mechanical properties of the biomaterials were evaluated by tensile test using Dumbbell's specimens of 25 mm ± 0.5 according to the standard ISO 37:2017 [53] with a load cell of 2 kN and a crosshead speed of 2.5 mm/min, *i.e.*, 10 % of strain rate. The ultimate tensile strength and elongation at break together with the Young's modulus were calculated averaging the results evaluated from the stress-strain curves. At least five specimen replicates, conditioned at room temperature (RT) and 54 % RH for 48 h, were tested at RT after 48 h from the extrusion, after 15 days and after one month of storage at room temperature.

2.7. Morphological characterization

The morphological analysis of the biomaterials was performed on cryo-fractured samples under liquid nitrogen. The fractured surface was then sputtered with a thin layer of gold, at 1.5 kV and 18 mA for 1 min. The samples were observed in an environmental scanning electron microscope PHILIPS XL3 FEG.

2.8. Release tests: simulant food

The release of OLE from the biomaterials was calculated according to the protocol of Nostro et al. [54] with few modifications. From injected specimens, 10 mm × 10 mm squares were cut to be used for release tests. Samples of approximately 11 ± 0.5 mg and 27 ± 0.5 mg for the biomaterials containing 10 wt% and 20 wt% of OLE, respectively, were immersed in 5 ml of distilled water and in a mixture of distilled water and ethanol (ethanol/water, 10:90), used as simulant food. The concentration of antioxidants released into the simulant was quantified using a Spectrophotometer UV–vis cary60 (Agilent Technologies) at 280 nm as reported in literature on the basis of standard curves (0–300 ppm) [46]. The release of OLE was corroborated at specific time intervals of 1, 3, 7, and 14 days and the amount of antioxidant released as polyphenols content was quantified from the absorbance curves using a standard curve of gallic acid, one of the most representative polyphenols in nature. The standard curve was obtained by measuring concentrations from 0 to 1000 mg/L of gallic acid using the Folin-Ciocalteu assay as reported by Di Meo et al. [30]. The equation of the line is as follows:

$$y = 0,001x$$

$$R^2 = 0,9583$$

Then the samples were immersed in 5 mL of fresh solvent. The cumulative release of OLE was calculated by sequentially sum of OLE released after each step.

2.9. Antioxidant activity (2,2-diphenyl-1-picrylhydrazyl – DPPH assay) and oxidation induction temperature (OIT)

Radical scavenging activity of the biomaterials containing OLE at initial and after the contact with food simulant [54] at different times (1, 3, 7, and 14 days) was determined by using a spectroscopic method according to the procedure proposed in literature [48,55,56], to test their effectiveness as active packages.

All solutions (50 μL) were mixed with 2.45 mL of DPPH in methanol (0.004 wt% methanol solution) and incubated at RT in the dark for 30 min. Then, the absorbance was measured at 517 nm using a UV/VIS spectrophotometer cary60 (Agilent Technologies). Methanol was used as blank. DPPH radical scavenging activity (RSA) was calculated according to the following Eq. (2):

$$RSA\% = \frac{(A_{DPPH} - A_{sample})}{A_{DPPH}} \cdot 100 \quad (2)$$

where, A_{DPPH} and A_{sample} are the absorbances at 517 nm of the DPPH solution and the sample under test, respectively.

The dynamic OIT test was performed by using the same DSC equipment described in the Section 2.4 and according to the ISO 11357-6:2018 standard "Plastics – Differential scanning calorimetry (DSC) – Part 6: Determination of oxidation induction time (isothermal OIT) and oxidation induction temperature (dynamic OIT)" [57]. Samples of around 5 mg were placed in an aluminium pan and subjected to the heating scan from room temperature until the oxidative reaction was displayed on the thermal curve under air atmosphere (50 mL/min) at a heating rate of 10 °C/min. The dynamic OIT was taken as the onset temperature of the exothermic oxidation of the materials.

2.10. Study of π-π stacking interactions

Fluorescence spectra of solid specimen and OLE, in powder form or in dimethyl sulfoxide (DMSO) solution, were recorded on a Horiba SPEX fluorolog 3 spectrometer using front-face setup (excitation and emission slits were varied between X-Y and W—Y nm, respectively, depending on emissivity of the sample). All the samples were excited at 350 nm based on their absorption spectra.

Attenuated total reflectance Fourier transform infrared (ATR-FTIR) spectra of the samples were acquired with a PerkinElmer FT-IR Spectrometer Frontier in ATR mode. 20 scans were performed from 4000 to 400 cm^{-1} with a resolution of 4 cm^{-1}. All data were treated using PerkinElmer Spectrum software.

3. Results and discussion

3.1. Chemical characterization of OLE

The composition of aqueous extract obtained from olive leaves by microwave extraction was reported in our previous work [30]. In brief, HPLC analysis revealed the presence of various polyphenolic components, phenolic acids and flavonoids, highlighting hydroxytyrosol (24 %) and oleuropein (46 %) as the main components [30].

Moreover, the composition of OLE was corroborated by ATR-FTIR, confirming the results obtained by HPLC. In fact, the ATR-FTIR spectra of OLE shows the typical bands observed in oleuropein and hydroxytyrosol (Fig. S.1 in Supporting information). The stretching vibration of hydroxyl groups in the O—H bond was observed at 3218 cm^{-1} while the bands in the range 3000–2800 cm^{-1} are representative of the asymmetric and symmetric stretching of CH_3 and CH_2 groups in long aliphatic chains [30]. Finally, the bands located between 1800 and 1500 cm^{-1} could be related to the stretching vibrations of C═O and C═C bonds typical of esters and carboxylic and phenolic acids. Moreover, the band at around 1600 cm^{-1} is representative of C—C aromatic stretching vibration confirming the presence of phenolic compounds [30].

3.2. Melt processing and visual aspect

PBAT/OLE biomaterials with or without CNC were successfully melt processed in a corotating twin screw micro-compounder and injected by using a micro injection moulding machine in different tests specimens, such as for Dynamic mechanical thermal analysis (DMTA) (Fig. 1). From the visual observation of the specimens, no visible CNC agglomerates nor OLE phase separation were detected. The addition of OLE alone or previously absorbed onto CNC resulted in a colour change, from white, typical of pristine and extruded neat PBAT, to brownish. The samples containing OLE were slightly more transparent than the samples containing CNC, due to the light scattering induced by the solid CNC as well as suggesting a nucleating effect of the nanocrystals.

3.3. Thermal analysis: TGA and DSC

Thermal stability of the biomaterials was analysed under inert atmosphere of nitrogen by thermogravimetric analysis and compared with the stability of OLE (Fig. 2, Table 2). The results show that OLE had a limited thermal stability with a $T_{5\%}$ and T_d at 163 °C and 184/264 °C, respectively, and a high tendency to charrification (34 % of char residue at 500 °C), according with previously reported data by Luzi et al. [48].

The onset of the thermal degradation of dried CNC was found at 222 °C and it shows three steps of degradation, a T_{d1} at 243 and 292 °C and a T_{d2} at 359 °C (Fig. 2, and Table 2). PBAT had an onset temperature at 359 °C and a maximum degradation temperature at 393 °C, indicating PBAT as a highly thermal stable thermoplastic polymer. PBAT led to an increase in the $T_{5\%}$ and in the T_d in all the biomaterials with respect to OLE alone, depending on the amount of OLE incorporated in the biomaterial. Indeed, 10-OLE-PBAT and 20-OLE-PBAT presented a $T_{5\%}$ of 283 and 243 °C respectively, and a T_d of 391 and 393 °C. This delay of the degradation onset and degradation temperature is retained also in aged samples (Fig. 2a–c, and Table 2), suggesting a good interaction between OLE and PBAT. PBAT delays also the degradation of CNC. In OLE-based biocomposites additional shoulders (230–330 °C) reflecting the presence of CNC are detectable. In aged biomaterials with 20 wt% of OLE, 20 degrees decrease in the degradation temperature to 371–369 °C points at a strong OLE PBAT interaction, which lead to a higher mobility of PBAT chains or phase separation, leading to faster thermal degradation.

To investigate the effect of both OLE and CNC on PBAT thermal properties, DSC analysis was carried out (Fig. 3, and Table 3). The DSC temperatures range was selected up to 160 °C based on a DSC analysis of the OLE extract, which was carried out instead up to 200 °C (Fig. S.2 in Supporting information). This analysis led to observe two melting peaks of OLE at ≈80 and 140 °C, while typical degradative signals are detected for temperatures higher than 160 °C, at variance with previous works

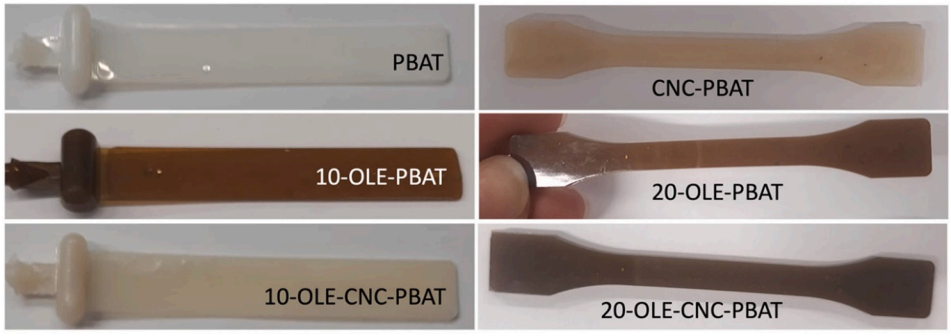

Fig. 1. Injected specimens of PBAT, CNC-PBAT, 10-OLE-PBAT, 10-OLE-CNC-PBAT, 20-OLE-PBAT, 20-OLE-CNC-PBAT. (For interpretation of the references to colour in this figure, the reader is referred to the web version of this article.)

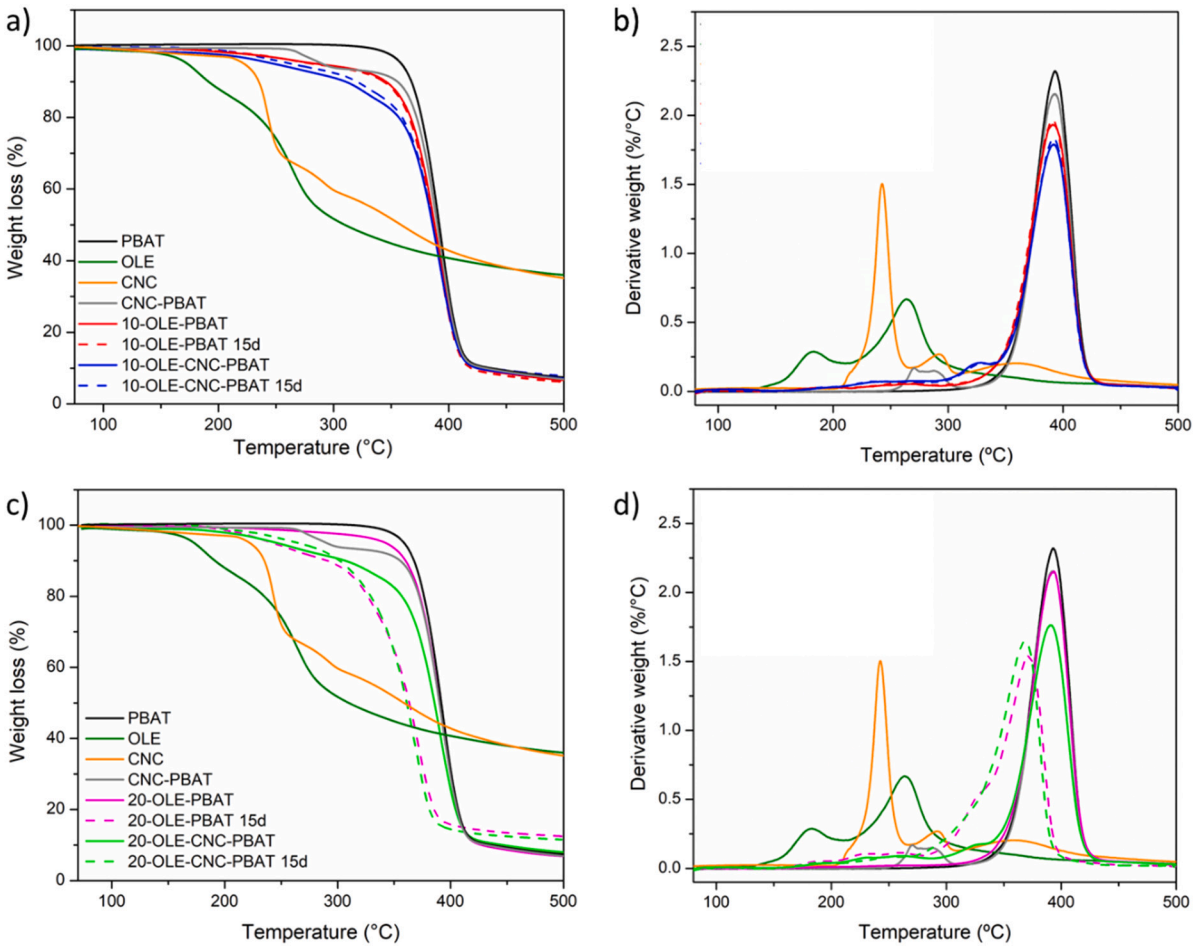

Fig. 2. Thermogravimetric curves (a, c) and their first derivative (b, d) of the biomaterials containing 10 wt% and 20 wt% of OLE with and without CNC, respectively.

Table 2
Main results from the thermogravimetric analysis: onset degradation temperature corresponding to the 5 % weight loss ($T_{5\%}$) and maximum degradation temperature as the peak of the thermogram derivative (T_d) of PBAT, OLE, CNC and the biomaterials just extruded and after storage for 15 days at room temperature in the dark, and char percentage at 500 °C. * Not detectable. Shoulder is reported between brackets.

Material	$T_{5\%}$ (°C)	T_{d1} (°C)	T_{d2} (°C)	Char residue at 500 °C (%)
PBAT	359	–*	393	7
OLE	163	182/264	–	34
CNC	222	243/292	359	33
CNC-PBAT	290	270–290	393	7
10-OLE-PBAT	283	–*	391	7
10-OLE-PBAT 15 d	281	–*	391	6
10-OLE-CNC-PBAT	248	(327)	391	7
10-OLE-CNC-PBAT 15 d	262	(329)	391	8
20-OLE-PBAT	243	–*	393	7
20-OLE-PBAT 15 d	241	(330)	371	12
20-OLE-CNC-PBAT	246	(328)	391	8
20-OLE-CNC-PBAT 15 d	265	(329)	369	12

reporting the melting temperature at about 175 °C for oleuropein, the main component of OLE [58,59]. These results are consistent with the observed initial degradative phenomena at 163 °C in the thermogravimetric analysis, and motivated the limitation of the selected DSC temperatures range up to 160 °C.

OLE did not significantly influence the PBAT glass transition and melting temperatures (T_g and T_m, respectively) in the biomaterials with 10 wt% and 20 wt% of OLE. T_m was about 126 °C, and the T_g was about −30/−32 °C, as for neat PBAT, and did not change over time for aged samples (Fig. 3b–d, and Table 3). However, OLE led to an increase in the crystallization temperature (T_c) for all the biomaterials from 82 °C to 90 °C with respect to the neat PBAT (Fig. 3a–c, and Table 3), indicating OLE nucleating effect on PBAT and the biocomposites.

The T_c of the biomaterials containing CNC showed also higher values, confirming a CNC nucleating effect.

Beber et al. [60] added polyhydroxybutyrate (PHB) and Babassu filler, a palm tree of Brazil which fruits are rich in lignin and cellulosic material, to PBAT to obtain novel film for food preservation obtaining a similar shift of the PBAT T_c. Carofiglio et al. [61] found the same results in a novel composites-based film with olive mill wastewater. In our study the T_c shifts with a slight increase compared to the PBAT and persists over time in all aged samples. Since the T_c values vary slightly over time, one could assume a good mixing of OLE with PBAT both alone and CNC-mixed. For 20-OLE-CNC-PBAT aged the increase in T_c is consistent with strong interaction between PBAT and OLE, or a minor phase separation, in agreement with the thermogravimetric analysis.

3.4. Morphology

To investigate the effect of the addition of OLE and the CNC to PBAT, a morphological analysis has been performed by scattering electron microscopy (Fig. 4). The PBAT morphology, at all magnifications, is consistent with a brittle surface fracture, typical of cryo-fractured PBAT.

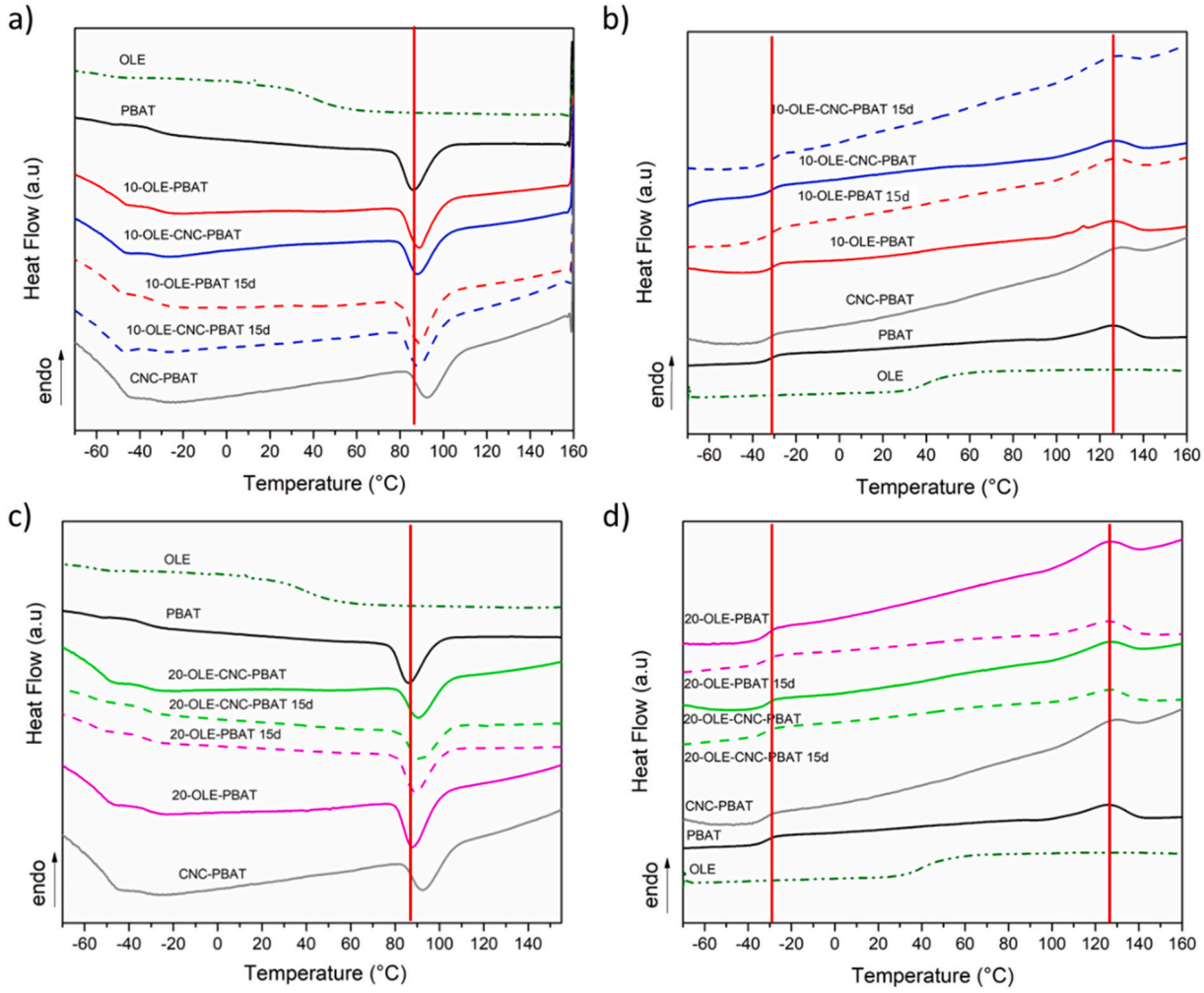

Fig. 3. DSC thermograms for PBAT and the biomaterials containing 10 wt% (a and b) and 20 wt% (c and d) of OLE and OLE-CNC: cooling scans (a and c) and second heating scans (b and d).

Table 3
Thermal properties of the biomaterials extrapolated from the second heating (glass transition T_g, melting T_m temperatures, and degree of crystallinity χ), and cooling scans (T_c). (–) Not detected.

Material	T_g (°C)	T_c (°C)	T_m (°C)	ΔH_m (J/g)	χ [%]
OLE	41	–	–	–	–
PBAT	−32	85	126	11	10
CNC-PBAT	−33	93	129	10	10
10-OLE-PBAT	−30	88	126	9	10
10-OLE-CNC-PBAT	−32	88	126	8	10
10-OLE-PBAT 15 d (aged for 15 days)	−31	89	126	10	10
10-OLE-CNC-PBAT 15 d (aged for 15 days)	−33	90	126	9	10
20-OLE-PBAT	−32	89	126	11	8
20-OLE-CNC-PBAT	−30	89	126	8	5
20-OLE-PBAT 15 d (aged for 15 days)	−32	88	126	10	7
20-OLE-CNC-PBAT 15 d (aged for 15 days)	−31	93	126	9	5

The addition of OLE slightly changes the PBAT morphology, but micrometric inclusions of a secondary phase are visible at higher magnifications, at 10 and 20 wt% of OLE, indicating a sporadic and limited phase separation. In the biocomposites, the mere addition of CNC lead to more irregular brittle fracture, and agglomerates CNC are distinguishable already at lower magnification. At higher magnifications, the CNC-PBAT biocomposites shows agglomerate of size larger than decades of microns, indicating a not uniform dispersion of CNC in the PBAT matrix.

The biocomposites prepared by the addition of 10 wt% of OLE and CNC show a morphology similar to the one shown by the neat PBAT at low magnification. This analysis is confirmed by the micrographs at higher magnifications, which show a uniform dispersion of CNC and few relatively small aggregates well embedded in the PBAT matrix. At higher OLE content the presence of micrometric holes is detected even at low magnification. In the higher magnified micrographs, a fine dispersion of CNC can be appreciated.

3.5. Mechanical properties

To evaluate the mechanical properties of the biomaterials the tensile tests were carried out at room temperature after conditioning for 72 h at 50 % RH all the sample. Representative stress-strain curves obtained are showed in Fig. 5 and the main results are summarized in Table 4.

At room temperature, over its glass transition (−32 °C), PBAT macromolecules are deformable because in their rubbery state. After the yield, they undergo to a strain hardening, due to an alignment of the PBAT macromolecules in the stress direction. PBAT peculiar tensile behaviour reflects the random copolymer structure of linear/aromatic randomly alternated segments, which undergo to progressive disentanglement of the polymer chains directly in strain hardening, and not

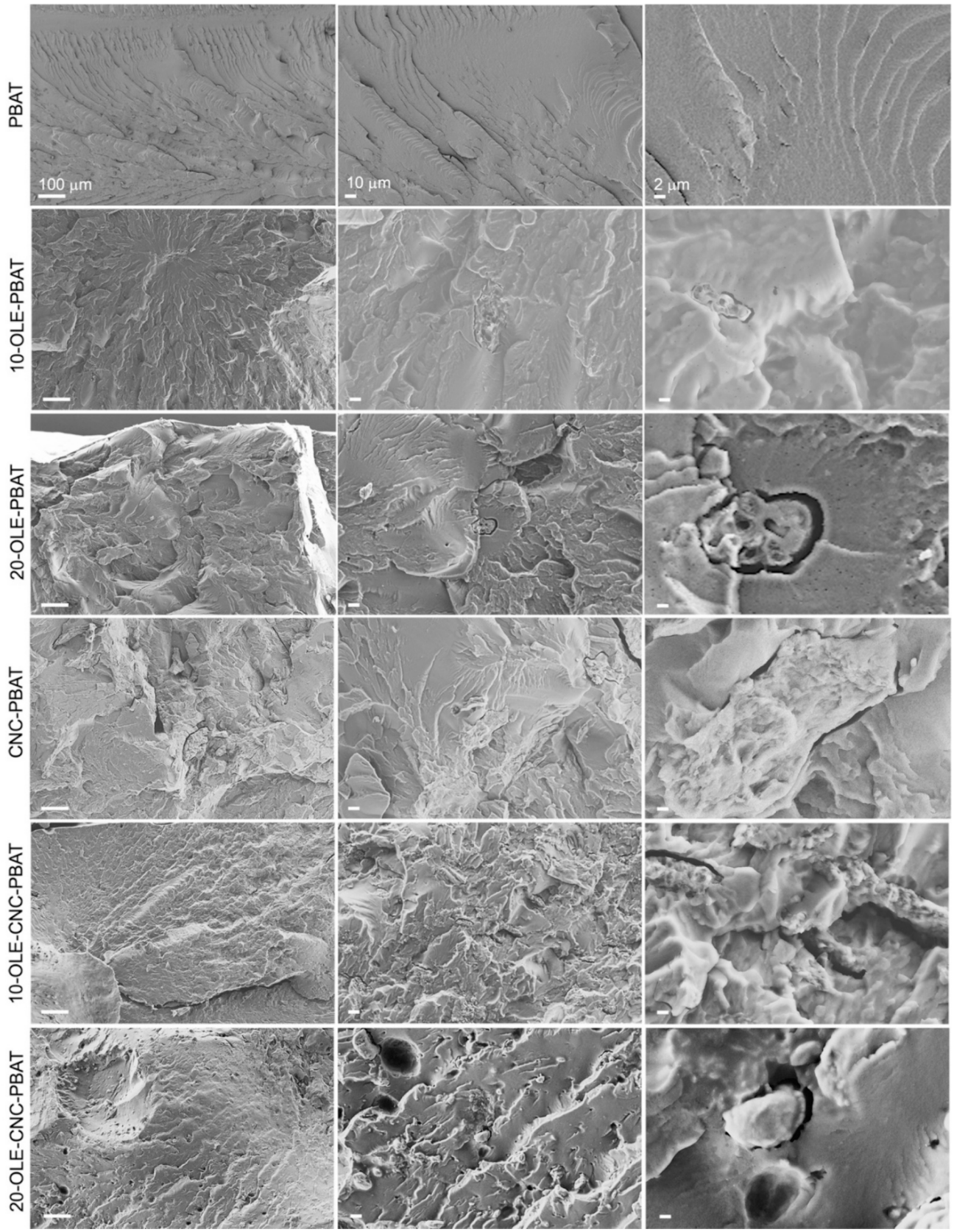

Fig. 4. Representative SEM micrographs of PBAT, 10-OLE -PBAT, 20-OLE- PBAT, CNC-PBAT, 10-OLE-CNC-PBAT and 20-OLE-CNC-PBAT at different magnifications (scale bars at 100, 10 and 2 µm from left to right).

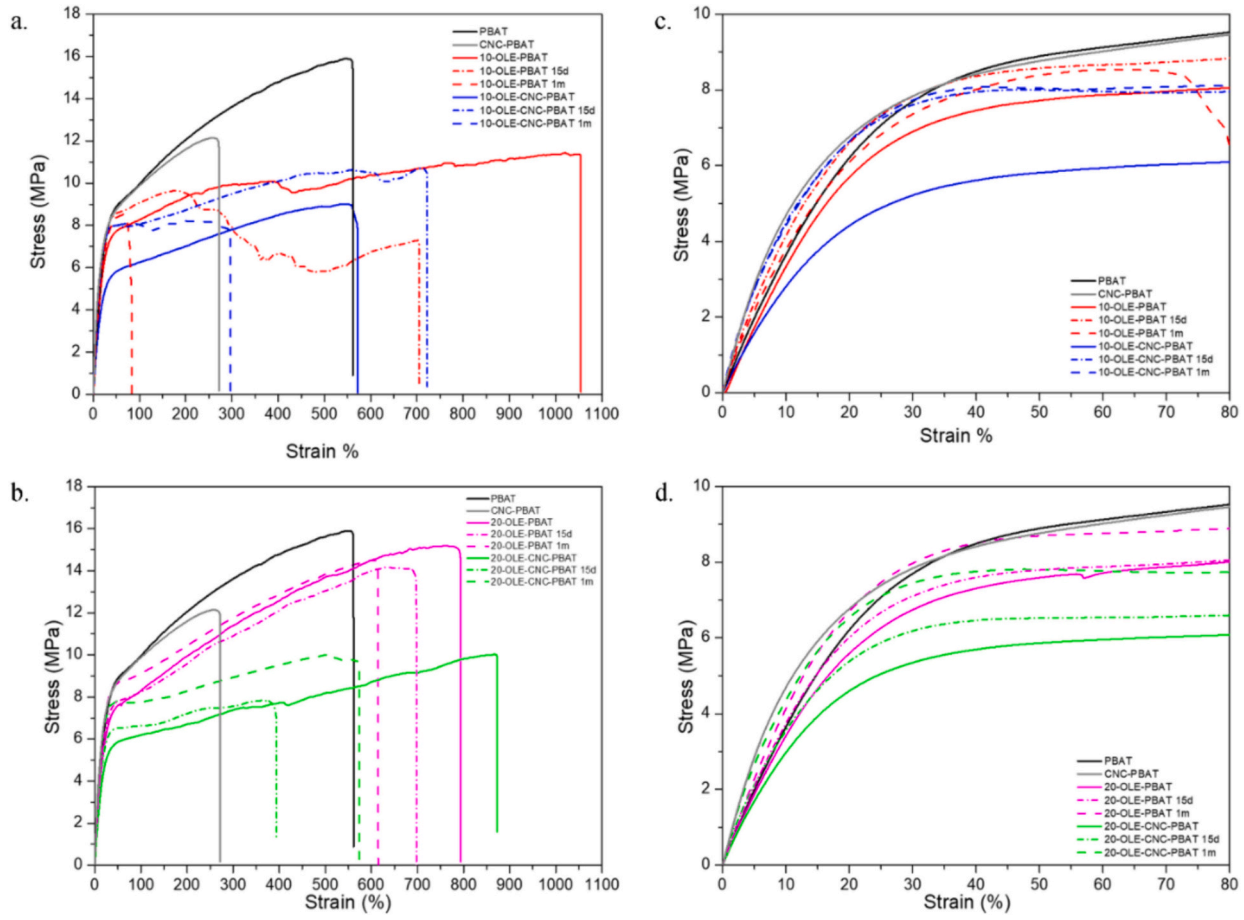

Fig. 5. Representative tensile behaviour and zoom in the elastic region of the tensile curve of PBAT, CNC-PBAT and biomaterials with 10 wt% (a and c) and 20 wt% of OLE (b and d) alone and OLE-CNC 15 d (aged for 15 days) and 30 d (aged for 30 days) after extrusion.

Table 4
Mechanical properties of the biomaterials.

Material	Young's modulus (MPa)	Ultimate strength (MPa)	Elongation at break (%)
PBAT	42 ± 3	16 ± 1	561 ± 56
CNC-PBAT	65 ± 3	12 ± 1	270 ± 56
10-OLE-PBAT	36 ± 4	12 ± 2	1053 ± 68
10-OLE-PBAT 15 d (aged for15 days)	54 ± 4	10 ± 1	704 ± 43
10-OLE-PBAT 30 d (aged for 30 days)	56 ± 2	9 ± 2	83 ± 63
10-OLE-CNC-PBAT	30 ± 2	9 ± 1	571 ± 53
10-OLE-CNC-PBAT 15 d (aged for 15 days)	64 ± 5	11 ± 2	721 ± 57
10-OLE-CNC-PBAT 30 d (aged for 30 days)	72 ± 3	8 ± 1	297 ± 73
20-OLE-PBAT	40 ± 4	15 ± 3	793 ± 48
20-OLE-PBAT 15 d (aged for 15 days)	44 ± 3	15 ± 2	697 ± 52
20-OLE-PBAT 30 d (aged for 30 days)	50 ± 3	15 ± 3	615 ± 49
20-OLE-CNC-PBAT	38 ± 5	10 ± 2	872 ± 66
20-OLE-CNC-PBAT 15 d (aged for 15 days)	45 ± 2	10 ± 1	594 ± 45
20-OLE-CNC-PBAT 30 d (aged for 30 days)	60 ± 3	10 ± 1	573 ± 65

showing the typical rubbery plateau of a linear semicrystalline thermoplastic polymer. Mean values of PBAT Young's modulus, ultimate strength, and elongation at break are about 42 MPa, 16 MPa, and 560 %, respectively. The addition of 10 wt% of OLE determined 88 % of increase in the PBAT elongation at break to 1050 %, and 17 % and 25 % of decrease in the PBAT Young's modulus and stress at break, respectively, highlighting the plasticizer effect of OLE.

The addition of 20 wt% of OLE to PBAT instead, maintained both PBAT stiffness and strength, only improving of over 40 % its deformability. These results indicate a good interaction between OLE and PBAT and an intimate level of OLE dispersion into PBAT matrix even when OLE reach the 20 wt% content, enabling higher mobility of its chains without a detrimental effect. Moreover, the tensile results indicate that the micrometric inclusions detected in the morphological analysis in the blends OLE/PBAT are not detrimental to the mechanical performance. This conclusion is further supported by the tensile behaviour of the aged materials, which show a progressive decrease in the tensile properties at 10 wt% of OLE content, while almost unchanged properties at 20 wt% OLE, even over a month.

The mere addition of CNC to PBAT, led to a stiffening and embrittlement of the matrix, with a 55 % increase of PBAT Young's modulus, and 25 and 52 % of decrease in PBAT stress and elongation at break, respectively. In the 10-OLE-CNC-PBAT biocomposite the presence of CNC halved the elongation at break, further decreasing the PBAT Young's modulus and stress at break, underlying the CNC inability to reinforce, while hindering the mobility of the PBAT chains. In the 20-OLE-CNC-PBAT biocomposite, the CNC led to a slight decrease of the Young's modulus and stress at break and an increase in the elongation at break, indication a plasticising effect of CNC, instead of a reinforcement effect. We have reported a similar behaviour of the same CNC in other deformable thermoplastic matrices [49], indicating a possible inclusion of redispersing agents such as polyethylene glycol in CelluForce CNC [62]. However, the ageing of this biocomposite progressively enhanced

the PBAT Young's modulus of about 43 %, while retaining the PBAT deformability. The ageing effect is ascribed to an improvement of the PBAT crystallinity over the time, induced by the higher mobility of PBAT chains gained by the good interaction and intimate dispersion of OLE, mediating the CNC/PBAT interface.

Scaffaro et al. [47] reported similar results in films containing nanoclay and carvacrol, a phenolic monoterpene contained in the essential oils of oregano and thyme. In fact, the tensile test performed using a first crosshead speed of 1 mm/min (for 3 min), and then increased to 100 mm/min, up to specimen failure, demonstrated that the elastic modulus and elongation at break of PBAT/PLA films containing 5 wt% of both nanoclay and carvacrol relatively incremented up to +70 % and +200 %, respectively, while retaining the same tensile strength of the neat matrix [47].

Overall, the tensile analysis indicates a beneficial effect of 20 wt% of OLE on PBAT, favouring the PBAT chains mobility which results in higher deformability and improving PBAT stiffness over the time. We can formulate a hypothesis of π-π staking interaction of OLE aromatic rings with the aromatic segments of PBAT, which lead to an effective OLE dispersion into the matrix, effect retained over time.

3.6. Release tests in food simulants and antioxidant properties

The release of OLE in food simulant solvents (water or ethanol/water mixture, 10:90) was evaluated by spectrophotometric measurements at 280 nm for 14 days. The results are expressed as the percentage of polyphenols measured in each time interval selected (Fig. 6). Biomaterials containing 10 wt% of OLE, with or without CNC, released the extract very quickly in both ethanol and water. Such a release took place from the first day of storage in food simulant solvents and reached values higher than 40 % in 14 days in both solvents.

The addition of 20 wt% of OLE to PBAT, instead, significantly affected the OLE release from the first day of immersion of the specimens in both simulants. In fact, even after 14 days the biomaterials released percentages lower than 5 % of extract in both simulant solvents. This result confirms a binding interaction between OLE and PBAT, probably ascribed to the π-π stacking interactions between the aromatic rings in OLE and the aromatic segments of PBAT, already suggested by the thermogravimetric and tensile analyses of 20-OLE-PBAT. Besides, when 20 wt% of OLE were added with CNC (20-OLE-CNC-PBAT) the release of the extract was higher (maximum 25 % after 14 days in both food simulants) compared to its counterpart without CNC (20-OLE-PBAT) but lower than the biomaterials containing 10 wt% of OLE. This difference is probably due to the existence of a competitive interaction (hydrogen bonding) between CNC and OLE in the biocomposite 20-OLE-CNC-PBAT, weakening the strong π-π stacking interactions between PBAT and OLE of the sample 20-OLE-PBAT.

Nostro et al. [54] demonstrated a slower release of citronellol from a poly(ethylene-*co*-vinyl acetate) (EVA) copolymer film filled with 3.5 wt % compared to 7 wt%. This is likely attributed to the hydrophobic nature of citronellol. In fact, when the essential oil content is increased to 7 wt%, the release occurs very rapidly during the first 48 h, suggesting that small natural molecules may have limited interaction with the polymers. In our case, OLE is characterized by the presence of larger molecules such as oleuropein, which also directly interacts with PBAT. As a result, the release in simulant food is slowed down when the material is loaded with a higher percentage of OLE.

In our study, the strategy to pre-absorbed OLE onto CNC was assessed with the aim to hinder the phase separation of OLE, and thus slowdown OLE release. The simulant food assays reveal that the OLE release in both simulants, EtOH/H_2O or only H_2O, is instead fastened by the presence of CNC at the day 1. The OLE release from 20-OLE-CNC-PBAT is lower than the 10 wt% of OLE-based material in ethanol-water and in water. However, 20-OLE-CNC-PBAT in both the simulants exhibits a higher release of OLE with respect to 20-OLE-PBAT, highlighting a detrimental interference of CNC in the OLE/PBAT interactions. Most probably, the pre-absorption of OLE onto CNC hinders the OLE to freely interact with PBAT chains.

As demonstrated in our previous work, OLE shows a strong antioxidant activity [30]. Therefore, inserting OLE into polymer matrices used for food packaging could contribute to the preservation of easily oxidizable and perishable foods such as fresh meat as also suggested by Luzi et al. [48]. To evaluate the antioxidant effect of the produced OLE-containing biomaterials at both 10 wt% and 20 wt%, with or without CNC, the solvents containing the OLE released during the release tests were analysed by DPPH assay at the time intervals of 1, 3, 7, and 14 days. Biomaterials containing 10 wt% of OLE had a significant antioxidant effect from the first day of storage (Fig. 7), consistently with the high OLE release after one day of release tests. To evaluate the significance of the antioxidant activity among the biomaterials and the control over time, two-way ANOVA statistical test was used. This test showed that 10-OLE-PBAT and 10-OLE-CNC-PBAT had a high antioxidant effect over the time (p-value 0,0001). The antioxidant effect is related to the release rate of the additive in both ethanol/water mixture and water. In particular, the biomaterials with 20 wt% of OLE exhibited a gradual release over time in water and water/ethanol 90:10.

The 20 wt% of OLE added to PBAT may result in antioxidant activity lasting for several days of storage and thus showing a potential effect in improving the shelf life of oxidizable foods. In fact, when 20-OLE-PBAT, was stored in water, the antioxidant activity started slowly from the day 3 and persisted significantly until day 14 (Fig. 6). In ethanol/water mixture there was a significant antioxidant activity from 1 day to 7 days

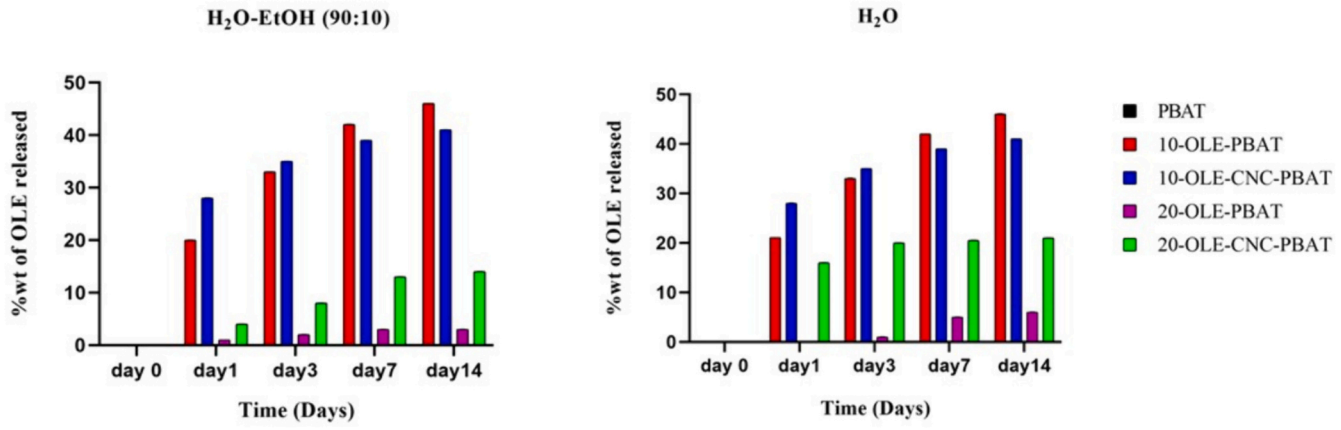

Fig. 6. Cumulative release expressed in percentage of polyphenols in simulant food solvent water or ethanol/water mixture (10:90) measured during 14 days of storage at RT by spectrophotometer absorbance at 280 nm.

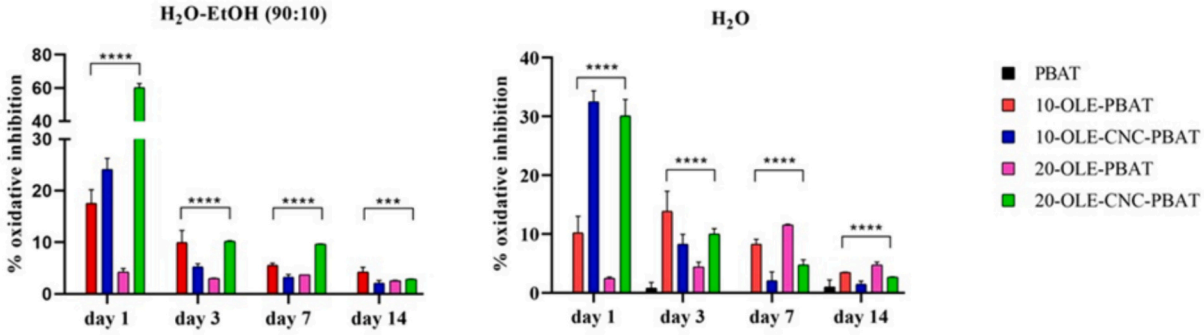

Fig. 7. Antioxidant activity measured using DPPH assay of biomaterials containing 10 wt% and 20 wt% of OLE, with or without CNC, in food simulant solvents recovered after release tests at the selected time intervals of 1, 3, 7, and 14 days. Statistical significance was examined by the two-way ANOVA test, with Dunnett's correction ($p < 0.05$) for bars comparison with control bar (PBAT). Asterisks indicate the statistical significance respect to the control (****$p < 0.0001$; ***$p < 0.001$; **$p < 0.01$; *p < 0.05); the absence of asterisks indicates absence of significance.

of storage as confirmed by the release rate reported in Fig. 6. 20-OLE-CNC-PBAT showed a higher antioxidant effect than 20-OLE-PBAT from day 1 to day 7 of storage, tending to decrease over time. Similar results were obtained by Luzi et al. [48] as well as by Nostro et al. [54] with two different polymeric films, poly(vinyl alcohol) (PVA) and EVA used for food packaging.

To further investigate the antioxidant effect of OLE on the oxidation process of PBAT, dynamic oxidation induction time (OIT) was evaluated by DSC. This test allows the relative measure of material's resistance to oxidative decomposition when subjected to a specified heating rate under air atmosphere. The dynamic OIT (Table 5) was determined by the calorimetric measurement of the onset temperature of the exothermic oxidation of the materials. The samples have been heated under air atmosphere up to 300 °C, to be sure to capture a thermo-oxidative degradation characterized by an exothermic peak during the test (Fig. 8).

Comparing the different curves, a similar trend was observed for 10-OLE-PBAT and 20-OLE-PBAT, for which the exothermic peak was not visible, indicating a delay of the oxidation reactions and a possible protective OLE role in PBAT oxidative degradation. Indeed, the beginning of the oxidative reaction was shifted throughout higher temperature when OLE was incorporated in the formulation as reported in Table 5. Adding 10 or 20 wt% of OLE, OIT values 60 and 70° higher than PBAT OIT were detected, respectively. In contrast, the mere addition of CNC decreased PBAT oxidative stability, indeed CNC-PBAT showed OIT values 10° lower then neat PBAT. Moreover, in the biocomposites, the stabilization effect of OLE was weaker than that in the biomaterials only containing OLE, probably due to the presence of CNC that weak the strong interaction between OLE and PBAT. Indeed, the OIT values of 10-OLE-CNC-PBAT and 20-OLE-CNC-PBAT were shifted of 23 and 30° higher than neat PBAT OIT, respectively. These results confirm that OLE can be applied as effective natural oxidative stabilizer for PBAT. In the literature, similar results were observed for cannabidiol [34], quercetin [33,63] and lignin [35].

Table 5
Dynamic oxidative-induction temperatures (OIT) values of PBAT and its blends with OLE and nano-composites with CNC.

Material	OIT (°C)
PBAT	208
CNC-PBAT	199
10-OLE-PBAT	268
10-OLE-CNC-PBAT	231
20-OLE-PBAT	278
20-OLE-CNC-PBAT	238

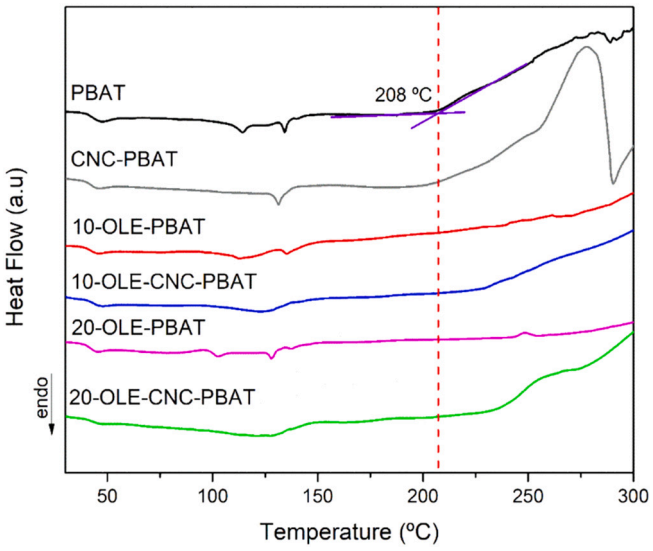

Fig. 8. Dynamic oxidative-induction temperatures (OIT) from DSC curves performed according to the ISO 11357-6:2018 standard of PBAT, OLE-based biomaterials and OLE-CNC biocomposites.

3.7. *Non-covalent interactions: π-π stacking experimental evidence*

The fluorescence behaviour of OLE was studied in solution (DMSO) and in solid state for the first time to our knowledge (Fig. 8). Both samples showed an emission band, one centred at around 433 and 474 nm for OLE in solution and in solid state, respectively. The latter showed a second band centred at around 587 nm.

These results highlight how the different conformation of the structure of OLE when in solution or in solid state affects the nature of the π-π stacking interactions; the emission band shifts and a second emission at higher wavelength appears. This effect has been already observed for other polyphenolic molecules, such as lignin by varying the solvent [64].

The emission band centred at 474 nm of OLE recorded in solid state appeared remarkably red-shifted (*i.e.*, shifted towards infrared frequencies in the tested frequencies range) in comparison with the emission band centred at 433 nm of OLE recorded in solution (Fig. 9a). This shift together with the appearance of the further band centred at 587 nm can be ascribed to the long-range intra-intermolecular π-π interactions formed during the solidification, where the degree of molecular order is higher, and the macromolecules are well packed and organized. The solubilization of OLE in DMSO weakened and/or released the non-covalent π-π stacking interactions at long-range, limiting the emission band to the fluorescence related to the aromatic rings in the solubilized

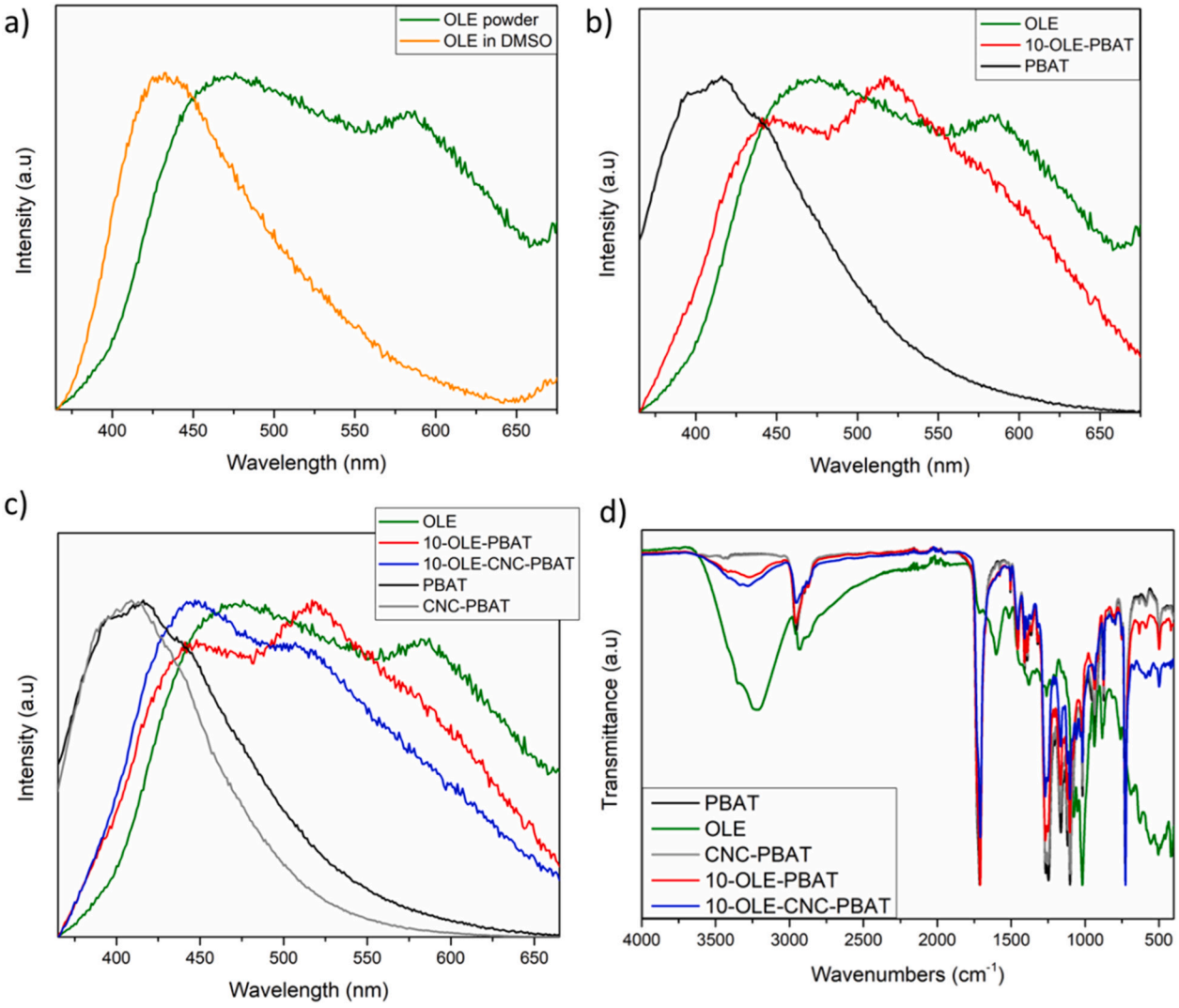

Fig. 9. Spectra of a) emission of OLE in solid state and in solution (DMSO), b) emission of neat PBAT, OLE and 10-OLE-PBAT in solid state, c) emission of neat PBAT, OLE, the reference CNC-PBAT and the 10 wt% OLE-based biomaterials in solid state, and d) ATR-FTIR of 10 wt% OLE-based biomaterials with or without CNC in solid state.

OLE, not supramolecularly organized. In the solid state also PBAT presented a relatively narrower band centred at λ_{em} between 400 and 425 nm, due to its organized aromatic segments (Fig. 9b). Comparing the fluorescence emitted from the solid biomaterials, 10-OLE-PBAT showed two broad emission bands centred at about 448 nm and 518 nm, emission bands blue-shifted towards higher frequencies when compared with the emission band of neat PBAT, and red-shifted compared to the emission bands presented by the solid OLE. The observed red-shifted wavelength in the biocomposite bands reflects the already described phenomena when OLE is dissolved in a solvent (DMSO). This reduction in the wavelength band demonstrates a less organized structure of OLE when dispersed in the polymeric matrix, due to reduced OLE intramolecular interactions, while OLE engages intermolecular non-covalent π-π staking with the aromatic domains of PBAT. On the other hand, the PBAT fluorescence band shifted to higher wavelength indicating a more organized interactions of the PBAT aromatic domains due to the presence of OLE, most probably acting as an attractor of these domains and boosting their organization upon solidification. These shifts confirm strong π-π stacking interactions between PBAT and OLE, which are prevalent compared to the pristine ones of neat OLE and neat PBAT, and further elucidate about the mechanisms of interactions between OLE and PBAT. Moreover, this analysis corroborates the mechanism of dispersion of OLE into PBAT and their miscibility. It is worth noting that this result is in line with the disappearance of the T_g of OLE in the thermograms of the biomaterials, pointing at a full miscibility between OLE and PBAT in the studied compositions. A similar behaviour was reported in literature for coumarin-based materials, pyrazoline materials [65] as well as for arylene ethynylene conjugated polyelectrolytes [66].

In contrast, the presence of CNC in PBAT-CNC and 10-OLE-CNC-PBAT did not significantly altered the emission band of the corresponding references PBAT and 10-OLE-PBAT, respectively (Fig. 9c). Only a 10 nm red-shift on the second emission band of 10-OLE-CNC-PBAT compared with 10-OLE-PBAT second emission band was registered. This effect could be due to hydrogen bonding interactions formed between CNC and OLE, which can be responsible of the disturb of CNC on the OLE/PBAT interactions discussed in the thermal and mechanical analyses. To further elucidate on the chemical interactions, ATR-FTIR spectra of the biomaterials and references were recorded (Fig. 9d). From the analysis of the spectra, it was possible to notice the disappearance of the band at 1600 cm^{-1} assigned to the ν O—H of OLE [67]. Even if by this analysis π-π interactions were not noticeable, the decreasing of the O—H band of OLE could be ascribed to the hydrogen bonding formed between CNC and OLE. Thus, these kinds of interactions

could compete with those between OLE and PBAT provoking a weakening of the intermolecular π-π stacking interactions.

4. Conclusions

PBAT/OLE biomaterials with or without CNC were successfully melt processed in a corotating twin screw micro-compounder and injected by using a micro injection moulding machine in the different test specimens. The thermogravimetric analysis indicates strong interaction between OLE and PBAT, which delays of >100° the OLE degradation in the biomaterials. Corroborated by the morphological analysis which indicate a homogeneous phase, the differential calorimetry indicates the presence of a unique glass transition in the biomaterials, demonstrating the full miscibility of OLE and PBAT. Moreover, this miscibility facilitated the CNC dispersion. Consistently, the tensile tests evidenced the role of OLE as plasticizer for PBAT providing higher values of elongation at break and indicate the 20 wt% OLE-based materials as the best formulations, enhancing the biomaterials deformability, limiting the decrease in Young's moduli and ultimate tensile strength, and stabilizing the biomaterials' performance also after ageing over a month.

Evaluating the simulant food test, the presence of 20 wt% of OLE in PBAT resulted in a decrease in OLE release in food simulant solvents (H_2O and EtOH 10 %). The results of the antioxidant activity test are consistent with the release study, confirming that the antioxidant activity of OLE is directly proportional to the amount of released polyphenols. 20-OLE-CNC-PBAT showed antioxidant activity from the first day of storage due to the faster release, while 20-OLE-PBAT retained the antioxidant effect for a longer time as the release was gradual.

The combination of OLE and CNC in the biocomposites does not lead to a synergistic effect on their properties. On the contrary, the presence of CNC seems to lower the favourable interaction between PBAT and OLE, inducing a slight ageing, thus to an embrittlement of the biocomposites after a month, and fasten the OLE release from the biocomposites.

All the results indicated strong interactions between OLE and PBAT, maximized at 20 wt% of OLE. The nature of these non-covalent interactions has been identified in π-π stacking bonds, by fluorescence spectroscopy. Already for 10-OLE-PBAT, this method highlighted the formation of π-π stacking between PBAT and OLE, by clear shifts of the emission bands of the pristine spectra.

Our results corroborate the incorporation of OLE in PBAT for food packaging with a stable mechanical performance and suggest its use at 20 wt% to exploit a persistent antioxidant activity.

CRediT authorship contribution statement

Giuseppa Anna De Cristofaro: Writing – original draft, Investigation, Formal analysis, Data curation. **Marina Paolucci:** Writing – review & editing, Validation, Supervision, Funding acquisition. **Daniela Pappalardo:** Writing – review & editing, Validation, Supervision, Formal analysis. **Caterina Pagliarulo:** Writing – review & editing, Validation, Supervision, Methodology. **Valentina Sessini:** Writing – review & editing, Validation, Supervision, Investigation, Formal analysis, Data curation. **Giada Lo Re:** Writing – review & editing, Validation, Supervision, Resources, Methodology, Investigation, Funding acquisition, Formal analysis, Data curation, Conceptualization.

Declaration of competing interest

The authors declare that they have no known competing financial interests or personal relationships that could have appeared to influence the work reported in this paper titled "Interface interactions driven antioxidant properties in olive leaf extract/cellulose nanocrystals/poly (butylene adipate-*co*-terephthalate) biomaterials".

Data availability

Data will be made available on request.

Acknowledgement

We would like to thank Oleificio Vascello S.a.s (Morcone, BN, Italy) for providing olive leaves used for experiments.

GLR acknowledges the Wallenberg Wood Science Center (WWSC) 2.0 program and Chalmers initiative GENIE for the financial support. VS would like to thank the Ministerio de Ciencia e Innovación (Spain) and the European Community (grant number: RYC2021-033921-I) and the University of Alcalá (PIUAH23/CC-046) for the financial support.

Appendix A. Supplementary data

Supplementary data to this article can be found online at https://doi.org/10.1016/j.ijbiomac.2024.132509.

References

[1] G. Forgione, F. Izzo, M. Mercurio, D. Cicchella, L. Dini, G. Giancane, M. Paolucci, Microplastics pollution in freshwater fishes in the South of Italy: characterization, distribution, and correlation with environmental pollutants, Sci. Total Environ. 864 (2023) 161032.
[2] B. Toussaint, B. Raffael, A. Angers-Loustau, D. Gilliland, V. Kestens, M. Petrillo, I. M. Rio-Echevarria, G. Van den Eede, Review of micro- and nanoplastic contamination in the food chain, Food Addit. Contam. Part A 36 (5) (2019) 639–673.
[3] C. Campanale, C. Massarelli, I. Savino, V. Locaputo, V.F. Uricchio, A detailed review study on potential effects of microplastics and additives of concern on human health, Int. J. Environ. Res. Public Health 17 (4) (2020).
[4] Z. Yuan, R. Nag, E. Cummins, Human health concerns regarding microplastics in the aquatic environment - from marine to food systems, Sci. Total Environ. 823 (2022) 153730.
[5] M.S. Bhuyan, Effects of microplastics on fish and in human health, Front. Environ. Sci. 10 (2022).
[6] T. Braun, L. Ehrlich, W. Henrich, S. Koeppel, I. Lomako, P. Schwabl, B. Liebmann, Detection of microplastic in human placenta and meconium in a clinical setting, Pharmaceutics 13 (7) (2021).
[7] E. Bioplastics, Bioplastics market data. https://www.european-bioplastics.org/market/, 2022.
[8] S. Mecking, Nature or petrochemistry?—biologically degradable materials, Angew. Chem. Int. Ed. 43 (9) (2004) 1078–1085.
[9] J. Jian, Z. Xiangbin, H. Xianbo, An overview on synthesis, properties and applications of poly(butylene-adipate-co-terephthalate)–PBAT, Adv. Ind. Eng. Polym. Res. 3 (1) (2020) 19–26.
[10] Statista, Distribution of the production capacities of bioplastics worldwide in 2021 and 2026, by material type. https://www.statista.com/statistics/678775/production-capacity-distribution-of-bioplastics-worldwide-by-material/, 2021.
[11] J. Šerá, M. Kadlečková, A. Fayyazbakhsh, V. Kučabová, M. Koutný, Occurrence and analysis of thermophilic poly(butylene adipate-co-terephthalate)-degrading microorganisms in temperate zone soils, Int. J. Mol. Sci. 21 (21) (2020) 7857.
[12] R. Muthuraj, M. Misra, A.K. Mohanty, Biodegradable compatibilized polymer blends for packaging applications: a literature review, J. Appl. Polym. Sci. 135 (24) (2018) 45726.
[13] M.G. Volpe, F. Siano, M. Paolucci, A. Sacco, A. Sorrentino, M. Malinconico, E. Varricchio, Active edible coating effectiveness in shelf-life enhancement of trout (Oncorhynchusmykiss) fillets, LWT Food Sci. Technol. 60 (1) (2015) 615–622.
[14] M.G. Volpe, M. Di Stasio, M. Paolucci, S. Moccia, Polymers for food shelf-life extension, Funct. Polym. Food Sci. (2015) 9–66.
[15] M. Giordano, C.G. Amoroso, C. El-Nakhel, Y. Rouphael, S. De Pascale, C. Cirillo, An appraisal of biodegradable mulch films with respect to strawberry crop performance and fruit quality, Horticulturae 6 (3) (2020) 48.
[16] E. Messinese, O. Pitirollo, M. Grimaldi, D. Milanese, C. Sciancalepore, A. Cavazza, By-products as sustainable source of bioactive compounds for potential application in the field of food and new materials for packaging development, Food Bioprocess Technol 17 (3) (2024) 606–627.
[17] C.J. Dillard, J.B. German, Phytochemicals: nutraceuticals and human health, J. Sci. Food Agric. 80 (12) (2000) 1744–1756.
[18] C. Leitzmann, Characteristics and health benefits of phytochemicals, Forsch. Komplementmed. 23 (2) (2016) 69–74.
[19] C.G. Fraga, K.D. Croft, D.O. Kennedy, F.A. Tomás-Barberán, The effects of polyphenols and other bioactives on human health, Food Funct. 10 (2) (2019) 514–528.
[20] S. Priya, P.K. Satheeshkumar, 5 - Natural products from plants: recent developments in phytochemicals, phytopharmaceuticals, and plant-based neutraceuticals as anticancer agents, in: B. Prakash (Ed.), Functional and Preservative Properties of Phytochemicals, Academic Press, 2020, pp. 145–163.

[21] A. Kumar, N. P, M. Kumar, A. Jose, V. Tomer, E. Oz, C. Proestos, M. Zeng, T. Elobeid, S. K, F. Oz, Major phytochemicals: recent advances in health benefits and extraction method, Molecules 28 (2) (2023).
[22] M.S. Mohd Basri, N.N. Abdul Karim Shah, A. Sulaiman, I.S. Mohamed Amin Tawakkal, M.Z. Mohd Nor, S.H. Ariffin, N.H. Abdul Ghani, F.S. Mohd Salleh, Progress in the valorization of fruit and vegetable wastes: active packaging, biocomposites, by-products, and innovative technologies used for bioactive compound extraction, Polymers 13 (20) (2021) 3503.
[23] A. Visco, C. Scolaro, M. Facchin, S. Brahimi, H. Belhamdi, V. Gatto, V. Beghetto, Agri-food wastes for bioplastics: European prospective on possible applications in their second life for a circular economy, Polymers 14 (13) (2022) 2752.
[24] M. Donner, I. Radić, Y. Erraach, F. El Hadad-Gauthier, Implementation of circular business models for olive oil waste and by-product valorization, Resources 11 (7) (2022) 68.
[25] I.O. Council, Yearly* olive oil production in Italy from 2005 to 2021. https://www.statista.com/statistics/710928/olive-oil-production-in-italy/, 2021.
[26] J. Espeso, A. Isaza, J.Y. Lee, P.M. Sörensen, P. Jurado, R.D.J. Avena-Bustillos, M. Olaizola, J.C. Arboleya, Olive leaf waste management, Front. Sustain. Food Syst. 5 (2021).
[27] A. Belščak-Cvitanović, K. Durgo, A. Huđek, V. Bačun-Družina, D. Komes, 1 - Overview of polyphenols and their properties, in: C.M. Galanakis (Ed.), Polyphenols: Properties, Recovery, and Applications, Woodhead Publishing, 2018, pp. 3–44.
[28] L.A.S. Cavaca, I.M. López-Coca, G. Silvero, C.A.M. Afonso, Chapter 5 - the olive-tree leaves as a source of high-added value molecules: oleuropein, in: R. Atta Ur (Ed.), Studies in Natural Products Chemistry, Elsevier, 2020, pp. 131–180.
[29] Z. Erbay, F. Icier, The importance and potential uses of olive leaves, Food Rev. Int. 26 (4) (2010) 319–334.
[30] a) M.C. Di Meo, G.A. De Cristofaro, R. Imperatore, M. Rocco, D. Giaquinto, A. Palladino, T. Zotti, P. Vito, M. Paolucci, E. Varricchio, Microwave-assisted extraction of olive leaf from five Italian cultivars: effects of harvest-time and extraction conditions on phenolic compounds and in vitro antioxidant properties, ACS Food Sci. Technol. 2 (1) (2022) 31–40;
b) M.C. Di Meo, F. Izzo, M. Rocco, A. Zarrelli, M. Mercurio, E. Varricchio, Mid-infrared spectroscopic characterization: new insights on bioactive molecules of *Olea europaea* L. leaves from selected Italian cultivars, Infrared Phys. Technol. 127 (2022) 104439.
[31] R. Imperatore, G. Orso, S. Facchiano, P. Scarano, S.H. Hoseinifar, G. Ashouri, C. Guarino, M. Paolucci, Anti-inflammatory and immunostimulant effect of different timing-related administration of dietary polyphenols on intestinal inflammation in zebrafish, *Danio rerio*, Aquaculture 563 (2023) 738878.
[32] V. Marturano, P. Cerruti, V. Ambrogi, Polymer additives, Phys. Sci. Rev. 2 (6) (2017).
[33] A. Masek, M. Latos, M. Piotrowska, M. Zaborski, The potential of quercetin as an effective natural antioxidant and indicator for packaging materials, Food Packag. Shelf Life 16 (2018) 51–58.
[34] A. Plota, A. Masek, Plant-origin stabilizer as an alternative of natural additive to polymers used in packaging materials, Int. J. Mol. Sci. 22 (8) (2021).
[35] L.B. Tavares, D.D.S. Rosa, Stabilization effect of kraft lignin into PBAT: thermal analyses approach, Matéria (Rio de Janeiro) 24 (2019).
[36] S.S. de Campos, A. de Oliveira, T.F.M. Moreira, T.B.V. da Silva, M.V. da Silva, J. A. Pinto, A.P. Bilck, O.H. Gonçalves, I.P. Fernandes, M.-F. Barreiro, F. Yamashita, P. Valderrama, M.A. Shirai, F.V. Leimann, TPCS/PBAT blown extruded films added with curcumin as a technological approach for active packaging materials, Food Packag. Shelf Life 22 (2019) 100424.
[37] J.C. Flores Fidelis, L.B. Marchi, M.R.S. Scapim, N.D. Gobetti, F. Yamashita, A. R. Giriboni Monteiro, Development of biodegradable films containing pomegranate peel extract and potassium sorbate, LWT 160 (2022) 113302.
[38] P.S. Müller, D. Carpiné, F. Yamashita, N. Waszczynskyj, Influence of pinhão starch and natural extracts on the performance of thermoplastic cassava starch/PBAT extruded blown films as a technological approach for bio-based packaging material, J. Food Sci. 85 (9) (2020) 2832–2842.
[39] S. Roy, J.-W. Rhim, Curcumin incorporated poly(butylene adipate-co-terephthalate) film with improved water vapor barrier and antioxidant properties, Materials 13 (19) (2020) 4369.
[40] X. Zhai, M. Li, R. Zhang, W. Wang, H. Hou, Extrusion-blown starch/PBAT biodegradable active films incorporated with high retentions of tea polyphenols and the release kinetics into food simulants, Int. J. Biol. Macromol. 227 (2023) 851–862.
[41] A.K. Rana, E. Frollini, V.K. Thakur, Cellulose nanocrystals: pretreatments, preparation strategies, and surface functionalization, Int. J. Biol. Macromol. 182 (2021) 1554–1581.
[42] N. Lin, J. Huang, A. Dufresne, Preparation, properties and applications of polysaccharide nanocrystals in advanced functional nanomaterials: a review, Nanoscale 4 (11) (2012) 3274–3294.
[43] S.S. Ahankari, A.R. Subhedar, S.S. Bhadauria, A. Dufresne, Nanocellulose in food packaging: a review, Carbohydr. Polym. 255 (2021) 117479.
[44] D.R. Shankaran, Chapter 14 - cellulose nanocrystals for health care applications, in: S. Mohan Bhagyaraj, O.S. Oluwafemi, N. Kalarikkal, S. Thomas (Eds.), Applications of Nanomaterials, Woodhead Publishing, 2018, pp. 415–459.
[45] M.B. Noremylia, M.Z. Hassan, Z. Ismail, Recent advancement in isolation, processing, characterization and applications of emerging nanocellulose: a review, Int. J. Biol. Macromol. 206 (2022) 954–976.
[46] B. Marcos, C. Sárraga, M. Castellari, F. Kappen, G. Schennink, J. Arnau, Development of biodegradable films with antioxidant properties based on polyesters containing α-tocopherol and olive leaf extract for food packaging applications, Food Packag. Shelf Life 1 (2) (2014) 140–150.
[47] R. Scaffaro, A. Maio, E.F. Gulino, M. Morreale, F.P. La Mantia, The effects of nanoclay on the mechanical properties, carvacrol release and degradation of a PLA/PBAT blend, Materials 13 (4) (2020) 983.
[48] F. Luzi, E. Pannucci, M. Clemente, E. Grande, S. Urciuoli, A. Romani, L. Torre, D. Puglia, R. Bernini, L. Santi, Hydroxytyrosol and oleuropein-enriched extracts obtained from olive oil wastes and by-products as active antioxidant ingredients for poly (vinyl alcohol)-based films, Molecules 26 (7) (2021) 2104.
[49] A. Venkatesh, L. Forsgren, A. Avella, K. Banke, J. Wahlberg, F. Vilaseca, G. Lo Re, A. Boldizar, Water-assisted melt processing of cellulose biocomposites with poly (ε-caprolactone) or poly(ethylene-acrylic acid) for the production of carton screw caps, J. Appl. Polym. Sci. 139 (6) (2022) 51615.
[50] G. Lo Re, V. Sessini, Wet Feeding Approach for Cellulosic Materials/PCL Biocomposites, Biomass Extrusion and Reaction Technologies: Principles to Practices and Future Potential, American Chemical Society, 2018, pp. 209–226.
[51] M.S.A. Avella, V. Sessini, R. Mincheva, G. Lo Re, Reusable, Recyclable and Biodegradable Heat-Shrinkable Melt Crosslinked PBAT/Pulp Biocomposites for PVC Replacement, 2023.
[52] F. Chivrac, Z. Kadlecová, E. Pollet, L. Avérous, Aromatic copolyester-based nano-biocomposites: elaboration, structural characterization and properties, J. Polym. Environ. 14 (4) (2006) 393–401.
[53] I.O.f. Standardization, ISO 37: 2017, Rubber, Vulcanized or Thermoplastic—Determination of Tensile Stress-Strain Properties, International Organization for Standardization, Geneva, Switzerland, 2017.
[54] A. Nostro, R. Scaffaro, M. D'Arrigo, L. Botta, A. Filocamo, A. Marino, G. Bisignano, Development and characterization of essential oil component-based polymer films: a potential approach to reduce bacterial biofilm, Appl. Microbiol. Biotechnol. 97 (21) (2013) 9515–9523.
[55] F. Luzi, E. Pannucci, L. Santi, J.M. Kenny, L. Torre, R. Bernini, D. Puglia, Gallic acid and quercetin as intelligent and active ingredients in poly(vinyl alcohol) films for food packaging, Polymers 11 (12) (2019) 1999.
[56] Y. Byun, Y.T. Kim, S. Whiteside, Characterization of an antioxidant polylactic acid (PLA) film prepared with α-tocopherol, BHT and polyethylene glycol using film cast extruder, J. Food Eng. 100 (2) (2010) 239–244.
[57] I.O.f. Standardization, ISO 11357-6, Plastics—Differential Scanning Calorimetry (DSC)—Part 6. Determination of Oxidation Induction Time (Isothermal OIT) and Oxidation Induction Temperature (Dynamic OIT), 2018.
[58] I. Mourtzinos, F. Salta, K. Yannakopoulou, A. Chiou, V.T. Karathanos, Encapsulation of olive leaf extract in β-cyclodextrin, J. Agric. Food Chem. 55 (20) (2007) 8088–8094.
[59] F. Flamminii, M. Paciulli, A. Di Michele, P. Littardi, E. Carini, E. Chiavaro, P. Pittia, C.D. Di Mattia, Alginate-based microparticles structured with different biopolymers and enriched with a phenolic-rich olive leaves extract: a physico-chemical characterization, Curr. Res. Food Sci. 4 (2021) 698–706.
[60] V.C. Beber, S. De Barros, M.D. Banea, M. Brede, L.H. De Carvalho, R. Hoffmann, A. R.M. Costa, E.B. Bezerra, I.D.S. Silva, K. Haag, K. Koschek, R.M.R. Wellen, Effect of Babassu natural filler on PBAT/PHB biodegradable blends: an investigation of thermal, mechanical, and morphological behavior, Materials 11 (5) (2018) 820.
[61] V.E. Carofiglio, P. Stufano, N. Cancelli, V.M. De Benedictis, D. Centrone, E. D. Benedetto, A. Cataldo, A. Sannino, C. Demitri, Novel PHB/Olive mill wastewater residue composite based film: thermal, mechanical and degradation properties, J. Environ. Chem. Eng. 5 (6) (2017) 6001–6007.
[62] P. Bourassa, M. Methot, R. Berry, Preparation of solvent and polymer redispersible formulations of dried cellulose nanocrystals (cnc), in: Google Patents, 2020.
[63] M.D. Samper, E. Fages, O. Fenollar, T. Boronat, R. Balart, The potential of flavonoids as natural antioxidants and UV light stabilizers for polypropylene, J. Appl. Polym. Sci. 129 (4) (2013) 1707–1716.
[64] M. Takada, Y. Okazaki, H. Kawamoto, T. Sagawa, Tunable light emission from lignin: various photoluminescence properties controlled by the lignocellulosic species, extraction method, solvent, and polymer, ACS Omega 7 (6) (2022) 5096–5103.
[65] V.F. Traven, D.A. Cheptsov, J.I. Svetlova, I.V. Ivanov, C. Cuerva, C. Lodeiro, F. Duarte, S.F. Dunaev, V.V. Chernyshev, The role of the intermolecular π···π interactions in the luminescence behavior of novel coumarin-based pyrazoline materials, Dyes Pigments 186 (2021) 108942.
[66] X. Zhao, M.R. Pinto, L.M. Hardison, J. Mwaura, J. Müller, H. Jiang, D. Witker, V. D. Kleiman, J.R. Reynolds, K.S. Schanze, Variable band gap poly(arylene ethynylene) conjugated polyelectrolytes, Macromolecules 39 (19) (2006) 6355–6366.
[67] S. Grabska-Zielińska, M. Gierszewska, E. Olewnik-Kruszkowska, M. Bouaziz, Polylactide films with the addition of olive leaf extract-physico-chemical characterization, Materials (Basel) 14 (24) (2021).